Chemical Physics Letters 493 (2010) 83–86

Contents lists available at ScienceDirect

Chemical Physics Letters

journal homepage: www.elsevier.com/locate/cplett

Low-temperature synthesis and structural properties of ferroelectric $K_3WO_3F_3$ elpasolite

V.V. Atuchin [a,*], T.A. Gavrilova [b], V.G. Kesler [c], M.S. Molokeev [d], K.S. Aleksandrov [d]

[a] Laboratory of Optical Materials and Structures, Institute of Semiconductor Physics, SB RAS, Novosibirsk 630090, Russia
[b] Laboratory of Nanolithography and Nanodiagnostics, Institute of Semiconductor Physics, SB RAS, Novosibirsk 630090, Russia
[c] Laboratory of Physical Principles for Integrated Microelectronics, Institute of Semiconductor Physics, SB RAS, Novosibirsk 630090, Russia
[d] Laboratory of Crystal Physics, Institute of Physics, SB RAS, Krasnoyarsk 660036, Russia

ARTICLE INFO

Article history:
Received 7 April 2010
In final form 6 May 2010
Available online 12 May 2010

ABSTRACT

Low-temperature ferroelectric G2 polymorph of $K_3WO_3F_3$ has been prepared by chemical synthesis. Structural and chemical properties of the final product have been evaluated with X-ray powder diffraction (XRD), scanning electron microscopy (SEM) and X-ray photoelectron spectroscopy (XPS). Structure parameters of G2–$K_3WO_3F_3$ are refined by the Rietveld method from XRD data measured at room temperature (space group *Cm*, $Z = 2$, $a = 8.7350(3)$ Å, $b = 8.6808(5)$ Å, $c = 6.1581(3)$ Å, $\beta = 135.124(3)$ Å, $V = 329.46(3)$ Å^3; $R_B = 2.47\%$). Partial ordering of oxygen and fluorine atoms has been found over anion positions. Mechanism of ferroelectric phase transition in $A_2BMO_3F_3$ oxyfluorides is discussed.

1. Introduction

Using asymmetric building blocks is an effective strategy for creation new noncentrosymmetric oxide compounds with such important physical properties as piezoelectricity, ferroelectricity and nonlinear optical effects [1,2]. From this point of view, transition metal oxyfluorides are very attractive because in this case the strong distortion of $[MO_{6-x}F_x]$ octahedrons is provided due to different ionicity of M–O and M–F bonds [3–5]. Topologically, the highest distortion of separated $[MO_{6-x}F_x]$ octahedron is achieved for $x = 3$ and such polar structural group seems be optimal for generation of low-symmetry complex compounds [6]. Indeed, several noncentrosymmetric inorganic crystals containing $[MO_3F_3]$ (M = Mo, W) groups were found by different research teams [6–9].

Oxyfluorides related to wide crystal family $A_2BMO_3F_3$ (A, B = Na, K, Rb, Cs; M = Mo, W) possess, with few exceptions, related structural, ferroelectric and ferroelastic properties within similar temperature intervals [10–14]. The temperatures of the ferroelectric (T_2) and ferroelastic (T_1) phase transitions detected in $A_2BMO_3F_3$ compounds are noticeably different. Cubic paraelectric phase G0 has been found for these compounds at $T > T_2$ [10,11]. For the representative member $K_3WO_3F_3$, the ferroelastic G2 ↔ G1 and ferroelectric G1 ↔ G0 transitions were found at $T_1 = 414$ K and $T_2 = 452$ K, respectively [10,11]. More recently, the values of T_1 and T_2 for the phase transitions in $K_3WO_3F_3$ were confirmed with structural and calorimetric measurements and Raman spectroscopy [13–15]. Unfortunately, the detailed information on the crystal structure of noncentrosymmetric G1 and G2 phases of $K_3WO_3F_3$ appeared at $T < 452$ K remains unknown up to now.

Several other compounds from $A_2BMO_3F_3$ family were studied with more details. Cubic structure with space group *Fm*3*m* was found for $Rb_2KMoO_3F_3$ above the $T_2 = 328$ K [9,11,16]. The noncentrosymmetric G1 phase with point group 3 over the temperature interval 182 K < T < 328 K and G2 phase with point group 3 or 1 at $T < T_1 = 182$ K were proposed initially [9,11]. Large spontaneous birefringence $\Delta n = 3.85 \times 10^{-3}$ ($\lambda = 542$ nm) and as high spontaneous polarization as $P_s = 30$ μC cm^2 were measured at $T = 300$ K for $K_3MoO_3F_3$ possessing $T_2 = 328$ K [17]. Detailed electron diffraction and XRD evaluation shown that symmetry of low-temperature ferroelectric polymorph G2 of $K_3MoO_3F_3$ at $T = 300$ K is monoclinic with space group *Ia* [18,19]. Triclinic space group *P*1 and $P_s = 0.021$ μC cm^2 were stated for the low-temperature G2 polymorph of $Na_3MoO_3F_3$ [20]. It has been shown that thallium oxyfluoromolybdate $Tl_3MoO_3F_3$ is also related to $A_2BMO_3F_3$ family, has two phase transitions at $T_2 = 315$ K and $T_1 = 403$ K and possesses monoclinic structure of low-temperature ferroelectric G2 polymorph with space group *Pa* [21]. Recently, a set of the phase transitions was observed in $A_2BMO_3F_3$, A = NH_4, compounds [22–26]. Accounting all presently available information on $A_2BMO_3F_3$ oxyfluorides it is evident that such cations as NH_4, Na, K, Rb, Cs and Tl may be considered at A and B positions in different combinations. However, crystal structure of ferroelectric G1 and G2 polymorphs, and respectively, a driving force of the phase transitions G2 ↔ G1 and G1 ↔ G0 is uncertain.

Present study is aimed to define the crystal structure of low-temperature ferroelectric G2–$K_3WO_3F_3$ polymorph to search for enabled lattice ordering. Assuming structural similarity between

* Corresponding author. Fax: +7 (3832) 332771.
E-mail address: atuchin@thermo.isp.nsc.ru (V.V. Atuchin).

0009-2614/$ - see front matter © 2010 Elsevier B.V. All rights reserved.
doi:10.1016/j.cplett.2010.05.023

G2 polymorphs of $A_2BMoO_3F_3$ (A, B = Na, K and Tl) and low-temperature state of $K_3WO_3F_3$, monoclinic or triclinic crystal structure can be supposed for G2–$K_3WO_3F_3$ phase. Respectively, very interesting combination of physical properties may be supposed for this ferroelectric $K_3WO_3F_3$ polymorph [27]. Earlier, high-temperature solid state synthesis or single crystal growth by Bridgman method were used for creation of $A_2BMO_3F_3$ compounds at $T \sim 900$–1100 K that is far above the ferroelectric transition temperature T_1 [8–12,16–21]. On cooling to room temperature the crystals were stressed by the phase transitions at T_1 and T_2. Low-temperature chemical synthesis from solutions was proposed for fabrication of ammonia-bearing oxyfluorides in G0 state [14,22–26]. In present study this method was developed to create directly the G2–$K_3WO_3F_3$ polymorph at the temperature below the T_2 boundary.

2. Experimental

Powder sample of $K_3WO_3F_3$ was fabricated by low-temperature chemical synthesis from water-based solutions. As starting reagents the KF (99.9%) and K_2WO_4 (99.5%) were used. At a first step a solution of potassium fluoride in hydrofluoric acid was prepared. After this, a solution of potassium tungstate in distilled water was carried out. Then, these two solutions were mixed with precautions because the reaction is active and with heating. As a result of reaction, white precipitate was separated out of the mother solution. After drying a white-colored powder product was formed.

Micromorphology of the crystals was evaluated by scanning electron microscopy (SEM) with the help of LEO 1430 device. Observation of electronic parameters of $K_3WO_3F_3$ was produced by using surface analysis center SSC (Riber) with X-ray photoelectron spectroscopy (XPS) method. The nonmonochromatic Al Kα radiation (1486.6 eV) with the power source of 300 W was used for the excitation of photoemission. The energy resolution of the instrument was chosen to be 0.7 eV, so as to have sufficiently small broadening of natural core level lines at a reasonable signal–noise ratio. Under the conditions the observed full width at half maximum (FWHM) of the Au $4f_{7/2}$ line was 1.31 eV. The binding energy (BE) scale was calibrated in reference to the Cu $3p_{3/2}$ (75.1 eV) and Cu $2p_{3/2}$ (932.7 eV) lines, assuring an accuracy of 0.1 eV in any peak energy position determination. Photoelectron energy drift due to charging effects was taken into account in reference to the position of the C 1s (284.6 eV) line generated by adventitious carbon present on the surface of the powder as-inserted into the vacuum chamber. Chemical composition was defined with using detailed spectra of K $3p_{3/2}$, W 4f, O 1s and F 1s core levels and known element sensitivity factors [28].

The powder X-ray diffraction pattern for Rietveld analysis was collected at room temperature (298 K) with a Bruker D8 ADVANCE diffractometer in the Bragg–Brentano geometry and linear Vantec detector. Operating parameters were: Cu Kα radiation, tube voltage 40 kV, tube current 40 mA, step size 0.016°, counting time 1s per step. The data were collected over the angle range 5–110°. Peak positions were determined with the program EVA, available in the PC software package DIFFRAC-PLUS supplied from Bruker. X-ray patterns of the title compound were indexed using the program McMaille [29].

3. Results and discussion

Fig. 1 demonstrates the SEM image of as-synthesized and dried potassium oxyfluorotungstate. The product has very uniform morphology with well coalescent nonfaceted microparticles. As it seems, crystal facet generation was precluded by enough high speed of reaction of precipitation. In Fig. 2 the survey photoemission spectrum recorded is presented. Besides constituent element core levels and Auger lines the low intensity signals of C 1s and Na 1s levels were detected. As it seems, the C 1s line is related to adventitious hydrocarbons captured by particle surface from air and sodium admixture is appeared due to traces in starting reagents. The representative constituent element core levels W $4f_{7/2}$, K $2p_{3/2}$, O 1s and F 1s indicate the BE values as 35.4, 292.6, 530.3 and 684.2 eV respectively. The BE value of the W $4f_{7/2}$ (35.4 eV) is within the range inherent for tungsten ions in the W^{6+} formal valence state in complex oxides [28,30–35]. The constituent element ratio estimated by XPS is K:W:O:F = 0.33:0.08:0.27:0.32 that is in close relation with nominal composition K:W:O:F = 0.30:0.10:0.30:0.30. It should be noted that the use of atomic sensitivity factors in the manner is normally furnishing semiquantitative results (within 10–20%) [28].

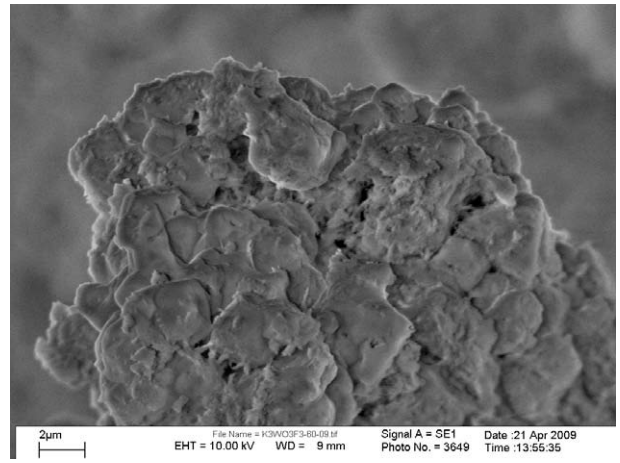

Fig. 1. Micromorphology of $K_3WO_3F_3$ particles.

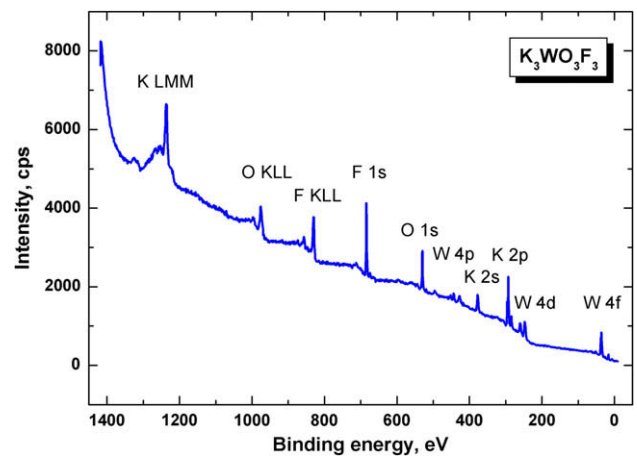

Fig. 2. Survey photoemission spectrum recorded for $K_3WO_3F_3$ sample.

Fig. 3 shows the XRD curve recorded for our powder sample. Only few low intensity peaks related to foreign phases were present in XDR curve related to $K_3WO_3F_3$. Crystal structure of $K_3WO_3F_3$ has been found at $T = 298$ K by Rietveld method ($R_B = 2.47\%$). The main parameters of processing and refinement are presented in Table 1. The potential space groups were defined by analysis of a systematic extinction of the reflections (*C*2, *Cm* or *C*2/*m*). The results were used as an input for the program FOX [36]. FOX uses global-optimization algorithms to solve the structure by performing trials in direct space. At first, the K atoms and WO_3F_3 octahedra were randomly placed in the unit cell. Then the agreement between measured and calculated diffraction patterns was maxi-

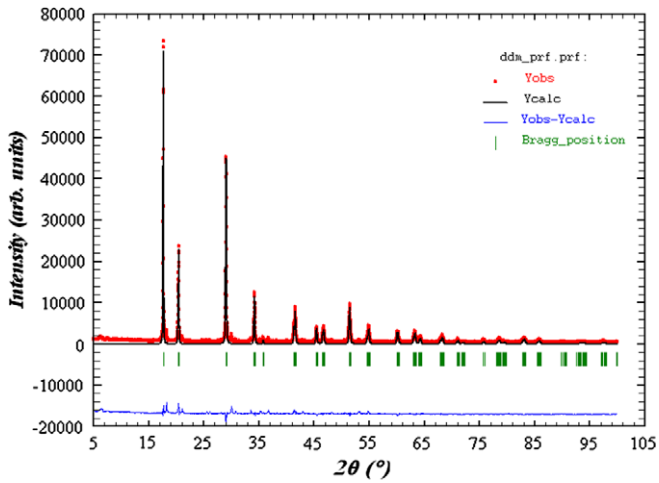

Fig. 3. Observed (red points) and calculated (black line) XRD patterns of monoclinic G2–$K_3WO_3F_3$. (For interpretation of the references to color in this figure legend, the reader is referred to the web version of this article.)

Table 1
The main parameters of processing and refinement.

Space group	*Cm*
a (Å)	8.7350 (3)
b (Å)	8.6808 (5)
c (Å)	6.1581 (3)
β (°)	135.124 (3)
Z	2
V (Å^3)	329.46(3)
2*θ*-interval range (°)	5–100
Number of reflexions	360
Number of refinement parameters	21
R_B	2.47%
R_{DDM}	9.73%
R_{wp}	19.18%

mized by using displacement and rotation of these atomic groups. All refinements and data processing have been performed by DDM program [37]. The Pearson VII function was used to model the peak profiles. The refinement of structure with *Cm* space group was stable and led to minimal R-factor in comparison with those for *C*2 and *C*2/*m* space groups. As a result, the space group *Cm* (No. 8) was selected for the low temperature phase of $K_3WO_3F_3$. The final refined atomic coordinates are given in Table 2 and metal–anion bond lengths and angles are given in Tables 3 and 4.

In G2–$K_3WO_3F_3$ crystal lattice all W atoms are in octahedral coordination and each W atom is surrounded by two O atoms, two F atoms and two mixed (O, F) positions. This complex coordination of W atoms in $K_3WO_3F_3$ is demonstrated in Fig. 4. So, calculated mean chemical bond length *L*(W–O) = 155.5 pm for the ordered oxygen positions is evidently shorter than *L*(W–F) = 202.5 pm for the ordered fluorine positions and [WO_3F_3] octahedron is strongly distorted. Two (O1, F1) positions remains to be disordered at room conditions and a potential for further polarization of [WO_3F_3] octahedrons is not exhausted.

It has been stated earlier that reversible phase transitions in $A_2BMO_3F_3$ oxyfluorides are associated with octahedral rotations and displacements of A and B cations [38]. Contrary to that, our structural results found for G2–$K_3WO_3F_3$ phase indicate the oxygen/fluorine ordering for two crystallographic positions. Complete oxygen/fluorine disorder was unambiguously obtained for high-temperature cubic G0 state of several $A_2BMO_3F_3$ phases [8–

Table 2
Fractional coordinates, occupancies (*p*) and isotropic atomic displacement parameters (B_i) for $K_3WO_3F_3$.

Atom	*x*	*y*	*z*	*p*	B_i (Å^2)
W	0	0	0	1.0	4.5 (1)
K1	−0.045 (9)	0.5	−0.07 (1)	1.0	10 (1)
K2	−0.002 (2)	0.731 (3)	0.461 (5)	1.0	2.8 (1)
F1	0.089 (6)	0.211 (4)	0.111 (6)	0.5	0.42 (3)
O1	0.089 (6)	0.211 (4)	0.111 (6)	0.5	0.42 (3)
F2	0.242 (7)	0	0.032 (1)	1.0	0.42 (3)
F3	0.763 (9)	0.5	0.472 (9)	1.0	0.42 (3)
O2	0.744 (9)	0	0.81 (1)	1.0	0.42 (3)
O3	0.426 (9)	0.5	0.70 (1)	1.0	0.42 (3)

Table 3
Selected bond distances for $K_3WO_3F_3$ at *T* = 298 K.

Bond	Length, Å
W–F1 (O1)	1.92 (3)
W–F2	1.99 (7)
W–F3	2.06 (3)
W–O2	1.48 (7)
W–O3	1.63 (7)
K1–F1 (O1)	2.66 (3)
K1–F2	2.3 (1)
K1–F3	2.02 (7)
K2–F1 (O1)	2.56 (5)
K2–F2	2.76 (3)
K2–F3	2.93 (7)
K2–O2	2.59 (3)

Table 4
Selected bond angles (°) for $K_3WO_3F_3$ at *T* = 298 K.

Atoms	Angle
O3–W–F1 (O1)	98.6 (8)
O3–W–O2	87 (3)
O2–W–F1 (O1)	105 (1)
O2–W–F2	153 (3)
O2–W–F3	126 (2)
F1(O1)–W–F1(O1)*	145 (1)
F1(O1)–W–F2	80 (1)
F1(O1)–W–F3	74.5 (7)
F2–K–F3	80 (2)

* A symmetry operation *x*, −*y*, *z* is used.

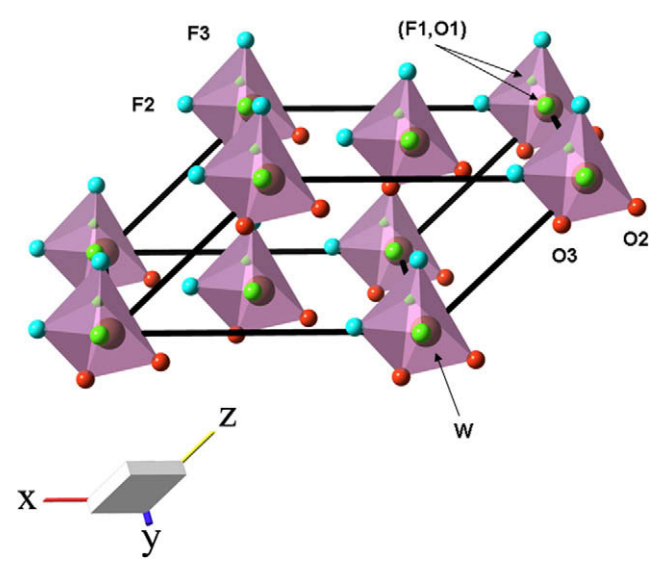

Fig. 4. Fragment of the crystal structure of room-temperature polymorph G2–$K_3WO_3F_3$. Oxygen, fluorine and mixed oxygen/fluorine positions are shown by red, blue and green colors, respectively. (For interpretation of the references to color in this figure legend, the reader is referred to the web version of this article.)

11,12,14,16,17,22–26]. Thus, as it appears, subsequent ordering of different oxygen/fluorine positions on cooling governs the nature of the phase transitions G0 → G1 → G2 in these oxyfluorides. Respectively, formation of one ordered oxygen/fluorine position can be supposed in ferroelectric G1 polymorph. Moreover, existence of a reversible phase transition G3 ↔ G2 between G2 and next completely ordered G3 polymorph can be proposed at very low temperature below a range of G2 polymorph.

4. Conclusions

The determination of structural parameters of G2–$K_3WO_3F_3$ polymorph gives an insight into mechanism of the phase transitions in $A_2BMO_3F_3$ oxyfluorides on cooling. Partial ordering of oxygen/fluorine positions is found and this seems be a cause of ferroelectric properties of G2 phase. Structural ordering is not finished in G2 polymorph and, respectively, one more phase transition is expected in $K_3WO_3F_3$ over the temperature range $0 < T < 300$ K.

References

[1] P. Shiv Halasyamani, Kenneth R. Poeppelmeier, Chem. Mater. 10 (1998) 2753.
[2] P. Shiv Halasyamani, Chem. Mater. 16 (2004) 3586.
[3] Kevin R. Heier, Alexander J. Norquist, P. Shiv Halasyamani, Angel Duarte, Charlotte L. Stern, Kenneth R. Poeppelmeier, Inorg. Chem. 38 (1999) 762.
[4] Michael R. Marvel, Julien Lesage, Jaewook Baek, P. Shiv Halasyamani, Charlotte L. Stern, Kenneth R. Poeppelmeier, J. Am. Chem. Soc. 129 (2007) 13963.
[5] Michael R. Marvel, Rachelle Ann F. Pinlac, Julien Lesage, Charlotte L. Stern, Kenneth R. Poeppelmeier, Z. Anorg. Allg. Chem. 635 (2009) 869.
[6] Paul A. Maggard, Tiffany S. Nault, Charlotte L. Stern, Kenneth R. Poeppelmeier, J. Solid State Chem. 175 (2003) 27.
[7] J. Ravez, J. Phys. III France 7 (1997) 1129.
[8] G. Péraudeau, J. Ravez, A. Tressaud, P. Hagenmuller, H. Arend, G. Chanussot, Solid State Commun. 23 (1977) 543.
[9] G. Péraudeau, J. Ravez, H. Arend, Solid State Commun. 27 (1978) 515.
[10] G. Peraudeau, J. Ravez, P. Hagenmuller, H. Arend, Solid State Commun. 27 (1978) 591.
[11] J. Ravez, G. Péraudeau, H. Arend, S.C. Abrahams, P. Hagenmuller, Ferroelectrics 26 (1980) 767.
[12] Jean-Pierre Chaminade[a], Manuel Cervera-Marzal[a], Jean Ravez[a], Paul Hagenmuller, Mater. Res. Bull. 21 (1986) 1209.
[13] I.N. Flerov, M.V. Gorev, V.D. Fokina, M.S. Molokeev, Ferroelectrics 346 (2007) 77.
[14] V.D. Fokina, I.N. Flerov, M.V. Gorev, M.S. Molokeev, A.D. Vasiliev, N.M. Laptash, Ferroelectrics 347 (2007) 60.
[15] A.A. Ekimov, A.S. Krylov, A.N. Vtyurin, A.A. Ivanenko, N.P. Shestakov, Ferroelectrics, 2010. doi: 10.1080/00150191003676280.
[16] S.C. Abrahams, J.L. Bernstein, J. Ravez, Acta Cryst. B 37 (1981) 1332.
[17] Z.G. Ye, J. Ravez, J.-P. Rivera, J.-P. Chaminade, H. Schmid, Ferroelectrics 124 (1991) 281.
[18] F.J. Brink, R.L. Withers, K. Friese, G. Madariaga, L. Norén, J. Solid State Chem. 163 (2002) 267.
[19] R.L. Withers, T.R. Welberry, F.J. Brink, L. Norén, J. Solid State Chem. 170 (2003) 211.
[20] Frank J. Brink, Lasse Norén, Darren J. Goossens, Ray L. Withers, Yun Liu, Chao-Nan Xu, J. Solid State Chem. 174 (2003) 450.
[21] F.J. Brink, L. Norén, R.L. Withers, J. Solid State Chem.174 (2003) 44.
[22] I.N. Flerov, M.V. Gorev, V.D. Fokina, A.F. Bovina, N.M. Laptash, Phys. Solid State 46 (2004) 915.
[23] Igor N. Flerov, Valentina D. Fokina, Asya F. Bovina, Nataliya M. Laptash, Solid State Sci. 6 (2004) 367.
[24] I.N. Flerov et al., Phys. Solid State 48 (2006) 106.
[25] I.N. Flerov, M.V. Gorev, V.D. Fokina, A.F. Bovina, M.S. Molokeev, E.I. Pogorel'tsev, N.M. Laptash, Phys. Solid State 49 (2007) 141.
[26] Yu.V. Gerasimova, A.S. Krylov, A.N. Vtyurin, A.A. Ivanenko, N.P. Shestakov, N.M. Laptash, Bull. Russ. Acad. Sci. 72 (2008) 1145.
[27] B.I. Kidyarov, V.V. Atuchin, Ferroelectrics 360 (2007) 96.
[28] C.D. Wagner, W.M. Riggs, L.E. Davis, J.F. Moulder, G.E. Muilenberg (Eds.), Handbook of X-ray Photoelectron Spectroscopy, Perkin-Elmer Corp., Phys. Elect. Div., Minesota, 1979.
[29] A. Le Bail, Powder Diffract. 19 (2004) 249.
[30] V.V. Atuchin, V.G. Kesler, N.Yu. Maklakova, L.D. Pokrovsky, Solid State Commun. 133 (2005) 347.
[31] O.Yu. Khyzhun, T. Strunskus, S. Cramm, Yu.M. Solonin, J. Alloys Compd. 389 (2005) 14.
[32] V.V. Atuchin, V.G. Kesler, N.Yu. Maklakova, L.D. Pokrovsky, D.V. Sheglov, Eur. Phys. J. B 51 (2006) 293.
[33] V.V. Atuchin, L.D. Pokrovsky, O.Yu. Khyzhun, A.K. Sinelnichenko, C.V. Ramana, J. Appl. Phys. 104 (2008) 033518.
[34] Yu-Xue Zhou, Hong-Bin Yao, Qiao Zhang, Yun-Yan Gong, Shu-Juan Liu, Shu-Hong Yu, Inorg. Chem. 48 (2009) 1082.
[35] S. Rajagopal, D. Nataraj, O.Yu. Khyzhun, Yahia Djaoued, J. Robinchaud, D. Mangalaraj, J. Alloys Compd. 493 (2010) 340.
[36] Vincent Favre-Nicolin, Radovan Cerny, J. Appl. Crystallog. 37 (2002) 734.
[37] L.A. Solovyov, J. Appl. Crystallog. 37 (2004) 743.
[38] Ray L. Withers, F.J. Brink, Yun Liu, Lasse Norén, Polyhedron 26 (2007) 290.